HHS Public Access

Author manuscript

Emergent Mater. Author manuscript; available in PMC 2026 March 07.

Published in final edited form as:

Emergent Mater. 2025 February ; 8(2): 1111–1120. doi:10.1007/s42247-024-00818-7.

Development of a 3D printed liquid-core hydrogel platform for real-time carbon nanotube sensors

Omer Sadak[1,2], **Mitchell A. Kuss**[3], **Wen Shi**[3], **Bin Duan**[3,4,5,6], **Nicole M. Iverson**[1]

[1]Biological Systems Engineering Department, University of Nebraska-Lincoln, Lincoln, NE, USA

[2]Department of Electrical and Electronics Engineering, Ardahan University, Ardahan, Turkey

[3]Mary and Dick Holland Regenerative Medicine Program, University of Nebraska Medical Center, Omaha, NE 68198, USA

[4]Division of Cardiology, Department of Internal Medicine, University of Nebraska Medical Center, Omaha, NE 68198, USA

[5]Department of Surgery, University of Nebraska Medical Center, Omaha, NE 68198, USA

[6]Department of Mechanical Engineering, University of Nebraska–Lincoln, Lincoln, NE 68588, USA

Abstract

Due to bioprinting technologies using a comparatively small amount of material, especially those that use print-on-demand techniques, they are considered to be promising production approaches. Though 3D bioprinting technologies are widely used in the creation of artificial tissues and organs, very little research has been done on their biosensor applications. Single-walled carbon nanotube (SWNT)-based optical sensors are highly praised for their remarkable sensitivity and specificity for a wide range of analytes. Nevertheless, due to the complexity of packaging and immobilization, problems continue to arise when incorporating SWNT sensors into both in vitro and in vivo applications. Herein, we report the use of 3D printing technology to improve SWNT sensor integration, resulting in adaptable and efficient platform designs. The optimized bioprinted hydrogel, composed of 3D-printable, modified Pluronic F-127, improves SWNT containment, ensuring stable fluorescence readings and increased fluorescence quenching in the presence of nitric oxide (NO). The hydrogel-encapsulated sensor maintains a ~95% fluorescence intensity over 90 days. Following the hydrogel parameter optimization, NO solutions were introduced to a 1.5-mm thick walled 30 mg/L SWNT-loaded hydrogel, revealing a gradual fluorescence intensity decrease with higher NO concentrations. Analysis shows a logarithmic relationship in the percentage of quenching at 990 nm within the concentration range of 1 μM to 50 μM, with the limit of detection (LOD) of 0.431 μM. When inserted under chicken skin, the sensor

Bin Duan, bin.duan@unmc.edu, Nicole M. Iverson, iverson@unl.edu.

Author contributions O.S: Investigation, Data curation, Validation, and Writing-Original draft preparation. Mitchell A.K: Conceptualization, Characterization, Methodology, Investigation, Validation, Writing, and Reviewing. W.S: Characterization, Data curation, Writing, and Reviewing. B.D: Conceptualization, Resources, Writing – review & editing, Supervision. N.M. I: Conceptualization, Resources, Writing – review & editing, Supervision.

Conflict of interest The authors declare no conflict of interest.

exhibits stable fluorescence readings, demonstrating its potential as a real-time in vivo sensor for minimally invasive health monitoring.

Keywords

Nitric oxide sensor; Bioprinting technologies; 3D printing technology; Single-walled carbon nanotube sensors; Liquid-core hydrogel

1 Introduction

The development of minimally invasive, real-time sensing platforms holds great promise in the field of medical technology, offering the potential to revolutionize the way we monitor human health [1–3]. 3D printing/bioprinting technologies, which deposit solution-based functional materials at desired locations with minimal processing steps, are one of the most promising production approaches for such advancements [4, 5]. Due to their efficient use of materials in the production process, the print-on-demand methods make these sensor technologies appealing. Limited research has been conducted on the biosensor applications of 3D printing/bioprinting technologies, despite their widespread utilization in the construction of engineered tissues and organs and therapeutic applications [6–11].

Optical sensors based on single-walled carbon nanotubes (SWNT) provide excellent specificity and sensitivity for identifying a wide range of analytes, including proteins, peptides, heavy metals, and small molecules [12–17]. However, difficulties in integrating them with packaging or immobilization approaches have limited their use in both in vitro and in vivo applications [18, 19]. SWNT sensors can be immobilized on/in a solid substrate, or they can be mixed directly with analyte solutions [17, 20, 21]. However, there are drawbacks to the direct mixing procedure, including the possibility of sample contamination and environmental or public health concerns [22, 23]. On the other hand, alternatives, such as confinement in a dialysis bag, surface immobilization on solid substrates (e.g., glass slides), and hydrogel encapsulation, can often be costly, unreliable, and inappropriate for use in resource-constrained environments [19, 24]. Therefore, investigating the incorporation of 3D printing technologies may present a viable way to address the difficulties encountered in effectively integrating SWNT sensors. These printing approaches have the potential to provide an efficient and adjustable sensor platform design, thereby reducing the limitations associated with traditional immobilization techniques [16, 25]. However, previous attempts to deliver SWNT sensors, even in large animal models, have encountered significant challenges that have limited their practicality and effectiveness. For example, Iverson et al. developed an alginate hydrogel containing SWNTs wrapped with a 28-nucleotide single-stranded DNA sequence $(AAAT)_7$, and it maintained its stability in a mouse model for 300 days after implantation. Due to interactions between the gel matrix and the ssDNA wrapping of the SWNT, the encapsulation changed the detection rate and recovery of the sensor while maintaining its specificity [26]. In another study, Hofferber et al. encapsulated SWNTs wrapped with $(AT)_{15}$, a 30-nucleotide single-stranded DNA sequence, in liquid core hydrogel and placed subcutaneously in wethers (< 1 year old male sheep) [20, 21]. Unfortunately, all of the liquid-core hydrogels broke during the 21-day period, likely due to

forces exerted on the hydrogel by the animals [20, 21]. Thus, a novel approach is needed to retain SWNT sensors within hydrogels without compromising specificity or altering detection rates and recovery.

The concentration of NO in biological systems can vary significantly depending on several factors, including the isoform of nitric oxide synthase (NOS) involved. The three NOS isoforms produce a wide range of NO concentrations, from nanomolar levels for neuronal NOS (nNOS) and endothelial NOS (eNOS) to micromolar levels for inducible NOS (iNOS) [27, 28]. While NOS was initially considered the primary source of NO, recent studies suggest that nitrite (NO_2^-) reduction also contributes to its biosynthesis [29, 30] Once generated, NO diffuses rapidly from its origin point, with an average lifetime ranging from milliseconds to seconds, reacting with and altering the function of various biomolecules. In vitro and in vivo NO levels have been reported to span from picomolar to micromolar concentrations, influenced by cell type, tissue type, NOS isoform expression, experimental conditions, and measurement techniques [31]. Given NO's significant involvement in physiological and pathological processes, particularly in cancer, it is crucial to monitor and quantify its concentration and dynamics to understand the disease mechanisms and advance therapeutic development [32, 33]. Therefore, a sensor that can detect NO from nanomolar to micromolar concentrations is highly desirable.

Herein, we developed and optimized a 3D printed liquid-core hydrogel platform that encapsulates the $(AT)_{15}$-wrapped SWNTs and studied its mechanical and optical characterizations. Notably, after 90-days at 37 °C, the fluorescence intensity exhibited a negligible decrease. Statistical analysis indicates that the change in intensity from day 1 to day 90 was statistically insignificant, highlighting the sensor's robust and stable performance over the extended testing period. A linear calibration curve was obtained when the percent quenching was plotted against the logarithm of the NO concentration. Furthermore, polyvinyl alcohol (PVA) wrapped SWNTs, a non-reactive control, that were incorporated into the 3D printed liquid-core hydrogel platform showed no quenching when they were exposed to NO. To investigate the burst resistance of the liquid-core hydrogel sensor, the mechanical properties were also assessed. Therefore, the 3D printed liquid-core hydrogel platforms have the potential for use as long-term in vivo sensors of small-molecule analytes, overcoming a major challenge in real-time medical diagnostics and monitoring.

2 Materials and methods

2.1 Materials

(6,5) Enriched Single-Wall Carbon Nanotubes (SWNT) (CoMoCAT), with a tube diameter ranging between 0.7 and 0.9 nm and a carbon content exceeding 93% were procured from Sigma Aldrich. The $(AT)_{15}$ single-stranded DNA was sourced from Integrated DNA Technologies in Iowa, USA. Sodium Hydroxide (NaOH), NaCl, Polyvinyl alcohol (PVA), and Sodium Cholate (SC) were purchased from Sigma Aldrich. Phosphate-buffered saline (PBS) and horseradish peroxidase were obtained from Thermo Fisher Scientific. Argon (99.999%), and NO gases were purchased from Matheson Tri-Gas, Inc. Fresh chicken skin was purchased from a local market and stored in a freezer at − 20 °C until further use. All aqueous solutions, unless specified otherwise, were prepared using nanopure water.

The Pluronic F-127 procured from Sigma Aldrich was modified using acrylic anhydride purchased from Combiblocks. For the hydrogel precursor additives, Lithium phenyl-2,4,6-trimethylbenzoylphosphinate (LAP) was purchased from Millipore-Sigma, tartrazine was obtained from Thermo Fisher Scientific, and the Omnirad 2959 (Irgacure 2959) was procured from IGM resins. A LumenX DLP 3D printer from Cellink was used for the 3D printing. An ultraviolet lamp from UVP (Upland, CA) was used to crosslink hydrogels for plugging the needle holes.

2.2 Synthesis of $(AT)_{15}$ and PVA wrapped-SWNT

$(AT)_{15}$-wrapped SWNT were prepared using a protocol published elsewhere [20, 34]. In brief, 2 mg mL^{-1} of $(AT)_{15}$ and SWNT (2:1 DNA: SWNT mass ratio) were added to 0.1 M NaCl solution. The solutions were bath-sonicated for 10-minutes (Bransonic, M2800H) before being ultrasonicated for 40-minutes with a 3 mm probe tip (QSonica Q125 Sonicator). Following two centrifugation cycles for 90-minutes, each time at 16,100 RCF, using an Eppendorf Centrifuge 5415D, the solution's supernatant was collected at the end of each cycle and kept at 4 °C.

PVA-wrapped SWNTs, also known as a non-reactive sensor, was synthesized as previously described [35]. Briefly, the SWNTs were ultrasonicated in a 2 w/v% sodium cholate (SC) solution for an hour in order to disperse them in SC. The resultant solution was centrifuged twice for 40 min each time at 16,100 RCF, with the pellet being removed at the end of each cycle. PVA was added to reach a final concentration of 2%. A 24-hour dialysis was performed on the resulting suspension against nanopure water. As previously reported, UV/vis spectrometry (Beckman Coulter DU730) was used to determine the concentration of the SWNT solutions.

2.3 Fabrication of liquid-core hydrogel

The liquid core-hydrogels were 3D printed using a modified Pluronic F-127. This 3D-printable Pluronic F-127 ink was modified and mixed using a previously reported protocol [36]. The ink contains 12.5% modified Pluronic F-127, 0.1 g/mL LAP photoinitiator diluted from a stock solution, and 1 mM tartrazine photoabsorber diluted from stock solution, all dissolved in water. They were printed using a LumenX DLP 3D printer (CellInk). The liquid-core hydrogels were 3D printed as hollow, pill-shaped constructs that are 6 mm in diameter and 12 mm long. The walls of the printed constructs are 1, 1.5–2 mm thick throughout the straight section and 2 mm on the rounded ends. This leaves a pill-shaped hollow inner core that is 3 mm in diameter and 8 mm long. One side of the construct contains a small, extended flat surface to serve as a base for the 3D printing (Fig. 1a, b and c). After printing, the constructs were briefly washed in water to remove excess ink and color and stored at room temperature in a moist environment.

2.4 SWNT injection into liquid-core hydrogel

First, the hydrogel was placed within a plastic container to keep it standing on the shorter end, allowing for increased stability of the hydrogel during injection. Subsequently, the excess liquid within the hydrogel was extracted using a syringe, while a needle was employed as a pressure regulator. Then the SWNT solution was injected into the hydrogel

while the needle was still in place. Upon completion of the injection process, the hydrogel was sealed by drop-casting of the modified pluronic F-127 dissolved in solution with Irgacure at the needle insertion sites, followed by exposure to UV light for 30 s. Video 1 illustrates the injection of SWNT sensors into the hydrogel. SWNT sensor-injected hydrogels were stored at room temperature under moist conditions until further use.

2.5 Mechanical characterization

The mechanical performance of the liquid-core hydrogel was performed on a CellScale® Univert Biomaterials Testing (CellScale, Canada) device with a cell load of 10 kg. Compression tests for 1, 1.5, and 2 mm thick SWNT-loaded liquid-core hydrogels were tested at strain rate of 0.2 mm/s with 10 consecutive compression cycles at a 40% compression strain.

2.6 Fluorescence measurements

A custom built nIR hyperspectral upright microscope (Photon, Etc. Montréal, Canada) modified with a 561 nm laser excitation source and an InGaAs camera array detector coupled with a volume Bragg grating to collect the sample emission was used to collect fluorescence measurements. The collected emission data were processed on PhySpec software (Photon Etc.), with subsequent post-processing of data performed using MATLAB.

The calibration curve was generated using an nIR spectrometer (B&W Tec) that utilized the mean fluorescence intensity. Samples were excited with a noncoherent light source (ThorLabs) through a liquid light guide equipped with a lowpass filter (900 nm cutoff) to minimize interference. The emitted light from the samples was gathered using a collimator linked to the nIR spectrometer via a fiber optic connection, maintaining a 180-degree angle between the collector and the light guide unless specified otherwise.

For accurate fluorescence measurements, the hydrogel was glued onto a petri dish via a topical skin adhesive-blue (Henry Schein, NY, USA). For optimization, the calibration curve, and quenching experiments, 3 mL of PBS was placed into the petri dish. For the fluorescence stability experiment, a 1.5 mm thick SWNT-loaded hydrogel was stored in normal saline (0.1 M NaCl) at 37 °C for 90 days in a sealed container.

For NO quenching experiments, NO gas was bubbled through nanopure water. Briefly, 15 mL of nanopure water in a sealed flask was first purged with Argon gas to deoxygenate the nanopure water for 20 min. Following this, NO was introduced into the flask for 5 min to generate the NO stock solution. The ultimate concentration of the NO was determined using the method outlined by Qiang et al. [37]. This NO solution was then combined with 1.36 μM horseradish peroxidase solution. The absorbance values at 405 and 420 nm were recorded and employed to calculate the NO concentration using Qiang et al.’s formula.

3 Results and discussion

For implantable hydrogel sensors, the mechanical properties, specifically recoverability and compressibility, are crucial for sustained, long-term measurements. To determine these characteristics, compression tests were conducted on hydrogels filled with nanopure water.

This approach served to assess the recoverability and compressibility of the prepared hydrogels. Instead of SWNT sensors, nanopure water was chosen due to concerns about potential environmental impact in case of hydrogel burst during experimentation. Figure 2a and b, and 2c show the representative images of the compressibility of 1-, 1.5-, and 2-mm thick liquid-core hydrogels, respectively. After 10 consecutive compression tests were performed at a 40% compression strain and a strain rate of 0.2 mm/s (Fig. 2d and e, and 2f), the hydrogels exhibited an excellent recoverability. As an example, 10 consecutive compression cycles of 1.5-mm thick liquid-core hydrogels are recorded (Video 2). Hydrogels created with similar components, but not with a liquid core, were previously studied by Duan's research group, and the bulk mechanical properties for the non-liquid core hydrogels were reported in Shi et al. [36]. Previous studies, along with our current liquid core data, demonstrate a robust hydrogel system that should remain stable under typical stress conditions.

Figure 1a and b, and 1c show a schematic of the 3D printed liquid-core hydrogel. The three different thicknesses used to optimize the parameters are shown. Figure 1d shows an example of a 1.5-mm thick and 30 mg/L of SWNT-loaded liquid core hydrogel, and its fluorescence image at 990 nm is shown in Fig. 1e. Individual fluorescence images were merged to form the integrated image, resulting in a pixelated appearance. Various amounts of $(AT)_{15}$-wrapped SWNT sensors (15, 30, 50, and 100 mg/L) were injected into the liquid-core hydrogels, and fluorescence readings were recorded. A linear relationship was observed between the concentration of the SWNT and the fluorescence intensity (Fig. 1f). Notably, no saturation was found at higher SWNT concentrations. As a result, all of the following measurements were carried out with a 30 mg/L SWNT solution to maintain consistency in our testing methodology.

It has been reported that SWNTs can pass or penetrate through physical barriers due to their small diameters [38]. Therefore, fluorescence intensities of 30 mg/L SWNT-loaded 1-, 1.5-, and 2-mm thick hydrogels were monitored for 4 h to assess their retention of the hydrogel. Prior to testing, the hydrogels were immersed in 3 mL of PBS at 37 °C within a petri dish for 15 min. In Fig. 3a, it is shown that the fluorescence intensity of 1-mm thick hydrogels exhibited the highest initial percent fluorescence intensity, but it diminished over the 4-hour period. Meanwhile, the 1.5-mm thick hydrogels displayed some fluctuations in fluorescence intensity but maintained their overall fluorescence for the entire 4 h. The 2 mm thick hydrogels showed a much lower initial fluorescence intensity but exhibited no significant change over time. The decrease in initial fluorescence intensity for the increasingly thick hydrogels is expected since the thicker hydrogels will decrease the excitation and emission signals. Considering their instability, the 1 mm-thick hydrogels were not employed in subsequent experiments.

The hydrogel core material, modified Pluronic F-127, used in our study is composed of a non-toxic, biocompatible, and biodegradable network [36, 39]. Specifically, the hydrogel is crosslinked using LAP to enhance the in vivo stability. These characteristics ensure that the hydrogel remains intact and stable within the intended biological environment. Although the 1 mm thick hydrogel showed the highest fluorescence intensity, we observed that the SWNT sensor was leaching from where it was injected. The observed decrease in the

fluorescence intensity in the 1 mm thick hydrogel can be attributed to technical challenges during the injection and sealing process. Specifically, the sealing agent did not adequately fill the hole in the capsule due to limitations imposed by the needle diameter and hydrogel thickness. Notably, this issue was not observed for the 1.5- and 2-mm thick hydrogels. Considering the application of the liquid-core hydrogel as a removable sensor could be a great approach to mitigate the risk of leaching and biodegradation. By designing the SWNT-based biosensor as a temporary, removable implant, we can avoid any long-term issues related to hydrogel degradation and sensor leaching. This approach ensures that the sensor can be safely retrieved after its intended use, providing a controlled and reliable method for in vivo monitoring without the risk of prolonged exposure.

The 30 mg/L SWNT-loaded 1.5-thick hydrogel was tested with the addition of 1 mL of 30 μM NO into the petri dish containing 3 mL of PBS solution, with 1 mL of PBS being removed before adding the stock solution. The 1.5-mm thick hydrogel exhibited a sharp decrease in fluorescence intensity upon the introduction of the NO solution, with a quick quenching time, as shown in Fig. 3b. This rapid quenching behavior in the 1.5-mm thick hydrogel is consistent with previous findings by Iverson's group, which observed similar behavior in thin layers of hydrogel and freely suspended SWNTs [40]. Given that the PBS solution in our experiments was not deoxygenated, the observed response indicates that NO gas likely permeated through the hydrogel before undergoing further reactions, in which it potentially forms NO_2. These findings underscore hydrogel's capability to detect NO gas and suggest its potential application in rapid-response sensing environments.

Previous studies had shown that when implanted under the skin in a mouse model, the composite hydrogels (Alginate/SWNT) remained stable for a period of 300 days [26]. Instead of performing a 300-day in vivo study, we simulated in vivo conditions for stability testing by submerging the liquid-core hydrogel platforms in normal saline (0.1 M NaCl) at 37 °C for 90 days. Following this 90-day period, there was no significant decrease in fluorescence intensity observed, as shown in Fig. 3c.

In contrast to $(AT)_{15}$-wrapped SWNTs, when electrostatically neutral PVA is wrapped onto SWNTs, it was reported that they showed no response to NO [41]. Given its lack of interaction with NO, the PVA-wrapped SWNT sensor can act as a control to demonstrate that the change in fluorescence intensity visualized for the $(AT)_{15}$-wrapped SWNTs upon addition the of NO is a result of the NO-SWNT interaction, not an unexpected reaction with the hydrogel components. We introduced 30 mg/L of the PVA/SWNT sensor into 1.5-mm thick liquid-core hydrogels and evaluated its response to NO, as demonstrated in Fig. 3d. Upon adding 30 μM NO to the sample, no fluorescence quenching was detected.

Following the optimization of the hydrogel parameters, various NO solutions were introduced to 1.5-mm thick 30 mg/L SWNT-loaded hydrogels. Fluorescence intensities were recorded from 900 to 1025 nm, as illustrated in Fig. 4a, using an nIR spectrometer. For this experiment, the same hydrogel sample was utilized throughout, and starting from lower concentrations, each concentration point was tested in 30-minute intervals. This interval was chosen considering the short half-life of NO and the hydrogel's rapid recovery, as demonstrated in Fig. 3b, to ensure minimal interference between consecutive data points. As

shown in the figure, the fluorescence intensity gradually decreased as higher concentrations of NO were added into the samples. The resulting data was used to create a concentration curve for NO quenching of the SWNTs by plotting the percent quenching at 990 nm against the varying concentrations of NO, revealing a logarithmic relationship, as depicted in Fig. 4b. The NO response, when plotted against the logarithm of the concentration, exhibited a well-fitted straight line, as presented in Fig. 4c. The derived equation for the fit is expressed as y (λ_{990}- λ_{922}) = 14.013 + 49.319 log (C (μM)) (R^2 = 0.983), where (λ_{990}- λ_{922}) represents the fluorescence peak intensity (%), and C denotes the added NO concentration (μM). Additionally, the limit of detection (LOD) was calculated by following the equation ($LOD = \frac{3\sigma}{S}$), where σ represents the standard deviation of the response at the lowest concentrations, and S is the slope of the calibration curve [42]. The LOD was determined to be 431 nM, which is within the biologically relevant range of NO concentrations. Future enhancements in the SWNT sensor, such as the chirality or length sorting of 6,5 SWNTs, could potentially lower the LOD, and improve the sensor's sensitivity toward detecting lower concentrations of NO.

As a proof of concept, SWNT-loaded hydrogels (concentration of 30 mg/L and measuring 1.5 mm in thickness) were placed between the skin and muscle tissue of a chicken breast, as depicted in Fig. 5a and b, and 5c. Fluorescent imaging was performed to demonstrate detection of the encapsulated SWNT through the layer of skin. A representative heatmap (Fig. 5d) shows the fluorescence of the SWNTs can be detected throughout the hydrogel, similar to what is observed without the layer of tissue (Fig. 1e). Moreover, no spectral shift was observed when the sensors were inserted into the tissue underneath the skin, as shown in Fig. 5e. However, a decrease in fluorescence intensity of about 74% was observed due to the tissue presence above the hydrogel. To assess whether the sensor remains functional under the skin, NO was introduced into the solution within a petri dish, resulting in a final NO concentration of 10 μM. Upon exposure to 10 μM NO, the hydrogel exhibited a decrease in fluorescence intensity over time, as shown in Fig. 5f. However, the quenching was not as rapid as what was observed in the control experiments conducted without the chicken skin (Fig. 3b). This difference suggests that the tissue layer affects the diffusion of NO into the hydrogel, thereby slowing the quenching process. The heat maps before, during, and after the quenching process are also illustrated in Fig. 5g and h, and 5i, respectively. This proof of concept provides promise of the in vivo usability of the SWNT-loaded hydrogel for monitoring NO concentrations in biological tissues.

4 Conclusions

In summary, this work highlights the potential of bioprinting technologies, particularly those that use print-on-demand processes, for biosensor applications. The integration difficulties related to SWNT-based optical sensors, which are known for their sensitivity and specificity, have been addressed through an innovative use of 3D printing technology. In addition to improving SWNT containment, the resulting bioprinted hydrogel provides stable fluorescence readings for 90 days and real-time fluorescence quenching in the presence of NO. After optimizing the parameters, the hydrogel platform showed a decrease in fluorescence intensity with increasing NO concentrations, allowing for the development

of a NO concentration curve. This logarithmic relationship in the percent of quenching ranges from 1 μM to 50 μM, with an LOD of 0.431 μM. Furthermore, the potential of the liquid-core hydrogel to be used as a real-time in vivo sensor for minimally invasive health monitoring is highlighted by its steady fluorescence measurements when placed beneath the skin of a chicken. This study offers a feasible and effective method for real-time monitoring in a variety of healthcare scenarios in addition to expanding our understanding of biosensor applications in bioprinting.

Supplementary Material

Refer to Web version on PubMed Central for supplementary material.

Acknowledgements

This work was supported by the Nebraska Research Initiative (NRI) Collaborative grant (project ID 32365) and the National Institute of Health (NIGMS) (1R35GM138245–01). The authors thank Trisam Sapkota from the University of Nebraska Lincoln for assisting with video editing and Dr. Eric Hofferber for his assistance on MATLAB codes for stitching images.

Data availability

The data that support the findings of this study are available from the corresponding author upon reasonable request.

References

1. Barhoum A, Sadak O, Ramirez IA, Iverson N, Stimuli-bioresponsive hydrogels as new generation materials for implantable, wearable, and disposable biosensors for medical diagnostics: principles, opportunities, and challenges. Adv. Colloid Interface Sci 317, 102920 (2023). 10.1016/j.cis.2023.102920 [PubMed: 37207377]
2. Yogev D, Goldberg T, Arami A, Tejman-Yarden S, Winkler TE, Maoz BM, Current state of the art and future directions for implantable sensors in medical technology: clinical needs and engineering challenges. Apl Bioeng. 7(3), 031506 (2023). 10.1063/5.0152290 [PubMed: 37781727]
3. Smith AA, Li R, Tse ZTH, Reshaping healthcare with wearable biosensors. Sci. Rep 13(1), 4998 (2023). 10.1038/s41598-022-26951-z [PubMed: 36973262]
4. Bozkurt Y, Karayel E, 3D printing technology; methods, biomedical applications, future opportunities and trends. J. Mater. Res. Technol 14, 1430–1450 (2021). 10.1016/j.jmrt.2021.07.050
5. Khan S, Ali S, Bermak A, Recent developments in Printing Flexible and Wearable Sensing Electronics for Healthcare Applications. Sens. (Basel) 19(5) (2019). 10.3390/s19051230
6. Russo V, Dickman CT, Jalili R, Campbell SA, Pan S, Hakimi N, Agarwal R, Yu Y, Khan K, Jahan K, Tong HH, Bedford E, Beyer S, Roos E, Mohamed T, Getsios S, Wadsworth S, Microfluidic 3D bioprinting: a Tool for developing tissue therapeutics. Tissue Eng. Pt A 28, 314–315 (2022)
7. Shi W, Mirza S, Kuss M, Liu B, Hartin A, Wan S, Kong Y, Mohapatra B, Krishnan M, Band H, Band V, Duan B, Embedded bioprinting of breast tumor cells and Organoids using low-concentration collagen-based Bioinks. Adv. Healthc. Mater 12(26), e2300905 (2023). 10.1002/adhm.202300905 [PubMed: 37422447]
8. Hockaday LA, Kang KH, Colangelo NW, Cheung PY, Duan B, Malone E, Wu J, Girardi LN, Bonassar LJ, Lipson H, Chu CC, Butcher JT, Rapid 3D printing of anatomically accurate and mechanically heterogeneous aortic valve hydrogel scaffolds. Biofabrication. 4(3), 035005 (2012). 10.1088/1758-5082/4/3/035005 [PubMed: 22914604]

9. Duan B, Hockaday LA, Kang KH, Butcher JT, 3D bioprinting of heterogeneous aortic valve conduits with alginate/gelatin hydrogels. J. Biomed. Mater. Res. A 101(5), 1255–1264 (2013). 10.1002/jbm.a.34420 [PubMed: 23015540]
10. Dias AD, Kingsley DM, Corr DT, Recent advances in bioprinting and applications for biosensing, Biosensors (Basel) 4(2) (2014) 111 – 36. 10.3390/bios4020111 [PubMed: 25587413]
11. Xu F, Moon S, Emre AE, Lien C, Turali ES, Demirci U, Cell bioprinting as a potential high-throughput method for fabricating cell-based biosensors (CBBs). Ieee Sens. 387–391 (2009). 10.1109/Icsens.2009.5398245
12. Wulf V, Bichachi E, Hendler-Neumark A, Massarano T, Leshem AB, Lampel A, Bisker G, Multicomponent System of Single-Walled Carbon Nanotubes Functionalized with a Melanin-Inspired Material for Optical Detection and Scavenging of Metals (Adv. Funct. Mater. 49/2022), Adv Funct Mater 32(49) (2022). 10.1002/adfm.202270281
13. Bisker G, Dong J, Park HD, Iverson NM, Ahn J, Nelson JT, Landry MP, Kruss S, Strano MS, Protein-targeted corona phase molecular recognition. Nat. Commun 7, 10241 (2016). 10.1038/ncomms10241 [PubMed: 26742890]
14. Kruss S, Salem DP, Vukovic L, Lima B, Vander Ende E, Boyden ES, Strano MS, High-resolution imaging of cellular dopamine efflux using a fluorescent nanosensor array. Proc. Natl. Acad. Sci. U S A 114(8), 1789–1794 (2017). 10.1073/pnas.1613541114 [PubMed: 28179565]
15. Zubkovs V, Schuergers N, Lambert B, Ahunbay E, Boghossian AA, Mediatorless, reversible Optical Nanosensor enabled through Enzymatic Pocket Doping. Small. 13(42) (2017). 10.1002/smll.201701654
16. Hofferber EM, Stapleton JA, Iverson NM, Review—single walled Carbon nanotubes as Optical Sensors for Biological Applications. J. Electrochem. Soc 167(3) (2020). 10.1149/1945-7111/ab64bf
17. Stapleton JA, Hofferber EM, Meier J, Ramirez IA, Iverson NM, Single-walled Carbon Nanotube Sensor platform for the study of Extracellular Analytes. Acs Appl. Nano Mater 4(1), 33–42 (2021). 10.1021/acsanm.0c01998 [PubMed: 34355133]
18. Iverson N, Barone P, Trudel L, Shandell M, Sen S, Sen F, Ivanov V, Atolia E, Farias E, McNicholas T, Reuel N, Parry N, Wogan G, Strano M, In vivo biosensing via tissue-localizable near-infrared-fluorescent single-walled carbon nanotubes. Abstr Pap Am. Chem. S 250 (2015)
19. Salem DP, Gong X, Liu AT, Akombi K, Strano MS, Immobilization and function of nIR-Fluorescent Carbon Nanotube sensors on Paper substrates for Fluidic Manipulation. Anal. Chem 92(1), 916–923 (2020). 10.1021/acs.analchem.9b03756 [PubMed: 31829619]
20. Hofferber E, Meier J, Herrera N, Stapleton J, Calkins C, Iverson N, Detection of single walled carbon nanotube based sensors in a large mammal. Nanomedicine. 40, 102489 (2022). 10.1016/j.nano.2021.102489 [PubMed: 34740870]
21. Hofferber E, Meier J, Herrera N, Stapleton J, Ney K, Francis B, Calkins C, Iverson N, Novel methods to extract and quantify sensors based on single wall carbon nanotube fluorescence from animal tissue and hydrogel-based platforms. Methods Appl. Fluoresc 9(2), 025005 (2021). 10.1088/2050-6120/abea07 [PubMed: 33631740]
22. Helland A, Wick P, Koehler A, Schmid K, Som C, Reviewing the environmental and human health knowledge base of carbon nanotubes. Environ. Health Perspect 115(8), 1125–1131 (2007). 10.1289/ehp.9652 [PubMed: 17687437]
23. Shvedova AA, Castranova V, Kisin ER, Schwegler-Berry D, Murray AR, Gandelsman VZ, Maynard A, Baron P, Exposure to carbon nanotube material: assessment of nanotube cytotoxicity using human keratinocyte cells. J. Toxicol. Environ. Health A 66(20), 1909–1926 (2003). 10.1080/713853956 [PubMed: 14514433]
24. Meier J, Stapleton J, Hofferber E, Haworth A, Kachman S, Iverson NM, Quantification of nitric oxide concentration using single-walled Carbon Nanotube Sensors. Nanomaterials (Basel). 11(1) (2021). 10.3390/nano11010243
25. Pan J, Li F, Choi JH, Single-walled carbon nanotubes as optical probes for bio-sensing and imaging. J. Mater. Chem. B 5(32), 6511–6522 (2017). 10.1039/c7tb00748e [PubMed: 32264414]
26. Iverson NM, Barone PW, Shandell M, Trudel LJ, Sen S, Sen F, Ivanov V, Atolia E, Farias E, McNicholas TP, Reuel N, Parry NM, Wogan GN, Strano MS, In vivo biosensing via tissue-

localizable near-infrared-fluorescent single-walled carbon nanotubes, Nat Nanotechnol 8(11) (2013) 873 – 80. 10.1038/nnano.2013.222 [PubMed: 24185942]

27. Gladwin MT, Schechter AN, Kim-Shapiro DB, Patel RP, Hogg N, Shiva S, Cannon RO, Kelm M, Wink DA, Espey MG, Oldfield EH, Pluta RM, Freeman BA, Lancaster JR, Feelisch M, Lundberg JO, The emerging biology of the nitrite anion. Nat. Chem. Biol 1(6), 308–314 (2005). 10.1038/nchembio1105-308 [PubMed: 16408064]
28. Pluth MD, Tomat E, Lippard SJ, Biochemistry of mobile zinc and nitric oxide revealed by fluorescent sensors. Annu. Rev. Biochem 80, 333–355 (2011). 10.1146/annurev-biochem-061009-091643 [PubMed: 21675918]
29. Bryan NS, Nitrite in nitric oxide biology: cause or consequence? A systems-based review. Free Radical Bio Med. 41(5), 691–701 (2006). 10.1016/j.freeradbiomed.2006.05.019 [PubMed: 16895789]
30. Timilsina A, Dong W, Hasanuzzaman M, Liu B, Hu C, Nitrate–nitrite–nitric oxide pathway: a mechanism of Hypoxia and Anoxia Tolerance in plants. Int. J. Mol. Sci 23(19), 11522 (2022) [PubMed: 36232819]
31. Alsharabasy AM, Aljaabary A, Bohara R, Farràs P, Glynn SA, Pandit A, Nitric Oxide-Scavenging, Anti-migration effects, and glycosylation changes after Hemin Treatment of Human Triple-negative breast Cancer cells: a mechanistic study. ACS Pharmacol. Translational Sci 6(10), 1416–1432 (2023). 10.1021/acsptsci.3c00115
32. Butler D, Sankhe CS, Khamsi PS, Gomez EW, Ebrahimi A, Solution-processed graphene films for electrochemical monitoring of extracellular nitric oxide released by breast cancer cells. 2D Mater. 11(1), 015021 (2024). 10.1088/2053-1583/ad1251
33. Lundberg JO, Weitzberg E, Nitric oxide signaling in health and disease. Cell. 185(16), 2853–2878 (2022). 10.1016/j.cell.2022.06.010 [PubMed: 35931019]
34. Ramirez IA, Sadak O, Sohail W, Huang X, Lu Y, Iverson NM, Development and evaluation of an expedited system for creation of single walled carbon nanotube platforms. Carbon Lett. (2024). 10.1007/s42823-024-00691-8
35. Giraldo JP, Landry MP, Kwak SY, Jain RM, Wong MH, Iverson NM, Ben-Naim M, Strano MS, A Ratiometric Sensor using single Chirality Near-Infrared fluorescent Carbon nanotubes: application to in vivo monitoring. Small. 11(32), 3973–3984 (2015). 10.1002/smll.201403276 [PubMed: 25981520]
36. Shi W, Jang S, Kuss MA, Alimi OA, Liu B, Palik J, Tan L, Krishnan MA, Jin Y, Yu C, Duan B, Digital Light Processing 4D Printing of Poloxamer Micelles for Facile fabrication of multi-functional biocompatible hydrogels as tailored wearable sensors. ACS Nano. 18(10), 7580–7595 (2024). 10.1021/acsnano.3c12928 [PubMed: 38422400]
37. Qiang L, Zhou J, Determination of nitric oxide using horseradish peroxidase by UV second-order derivative spectrometry. Anal. Sci 25(12), 1467–1470 (2009). 10.2116/analsci.25.1467 [PubMed: 20009336]
38. Zare H, Ahmadi S, Ghasemi A, Ghanbari M, Rabiee N, Bagherzadeh M, Karimi M, Webster TJ, Hamblin MR, Mostafavi E, Erratum: Carbon nanotubes: Smart Drug/Gene Delivery carriers [Corrigendum]. Int. J. Nanomed 16, 7283–7284 (2021). 10.2147/IJN.S338281
39. Diniz IMA, Chen C, Xu X, Ansari S, Zadeh HH, Marques MM, Shi S, Moshaverinia A, Pluronic F-127 hydrogel as a promising scaffold for encapsulation of dental-derived mesenchymal stem cells. J. Mater. Science: Mater. Med 26(3), 153 (2015). 10.1007/s10856-015-5493-4
40. Hofferber EM, Stapleton JA, Adams J, Kuss M, Duan B, Iverson NM, Implantable Nanotube Sensor Platform for Rapid Analyte Detection. Macromol. Biosci 19(6), e1800469 (2019). 10.1002/mabi.201800469 [PubMed: 30942955]
41. Zhang J, Boghossian AA, Barone PW, Rwei A, Kim JH, Lin D, Heller DA, Hilmer AJ, Nair N, Reuel NF, Strano MS, Single molecule detection of nitric oxide enabled by d(AT)15 DNA adsorbed to near infrared fluorescent single-walled carbon nanotubes, J Am Chem Soc 133(3) (2011) 567 – 81. 10.1021/ja1084942 [PubMed: 21142158]
42. Sadak O, Sundramoorthy AK, Gunasekaran S, Highly selective colorimetric and electrochemical sensing of iron (III) using Nile red functionalized graphene film, Biosens Bioelectron 89(Pt 1) (2017) 430–436. 10.1016/j.bios.2016.04.073 [PubMed: 27132997]

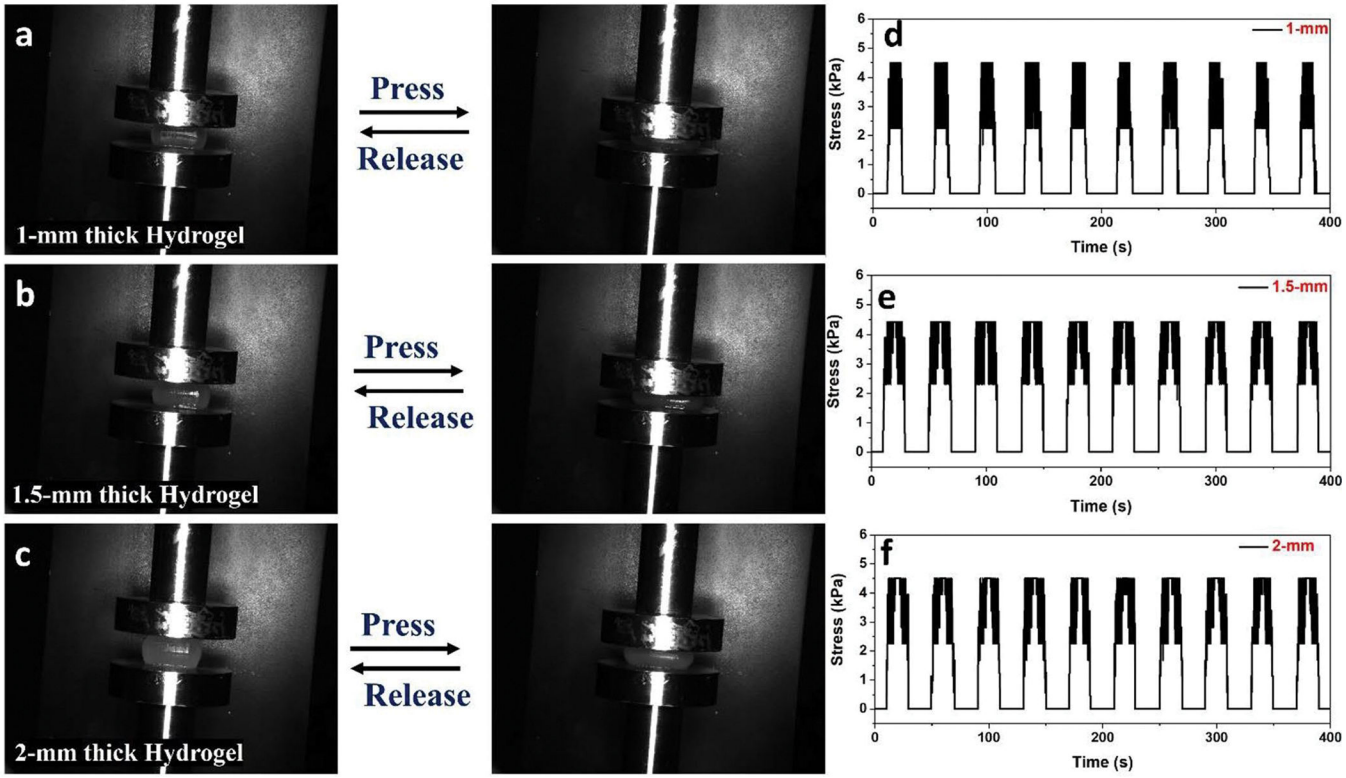

Fig. 1.

Representative photographs of (**a**) 1-mm, (**b**) 1.5-mm, and (**c**) 2-mm thick hydrogels before and during the 40% compression strain. Compressive cycle stability of (**d**) 1-mm, (**e**) 1.5-mm, and (**f**) 2-mm thick hydrogels at a 40% compression strain with a strain rate of 0.2 mm/s

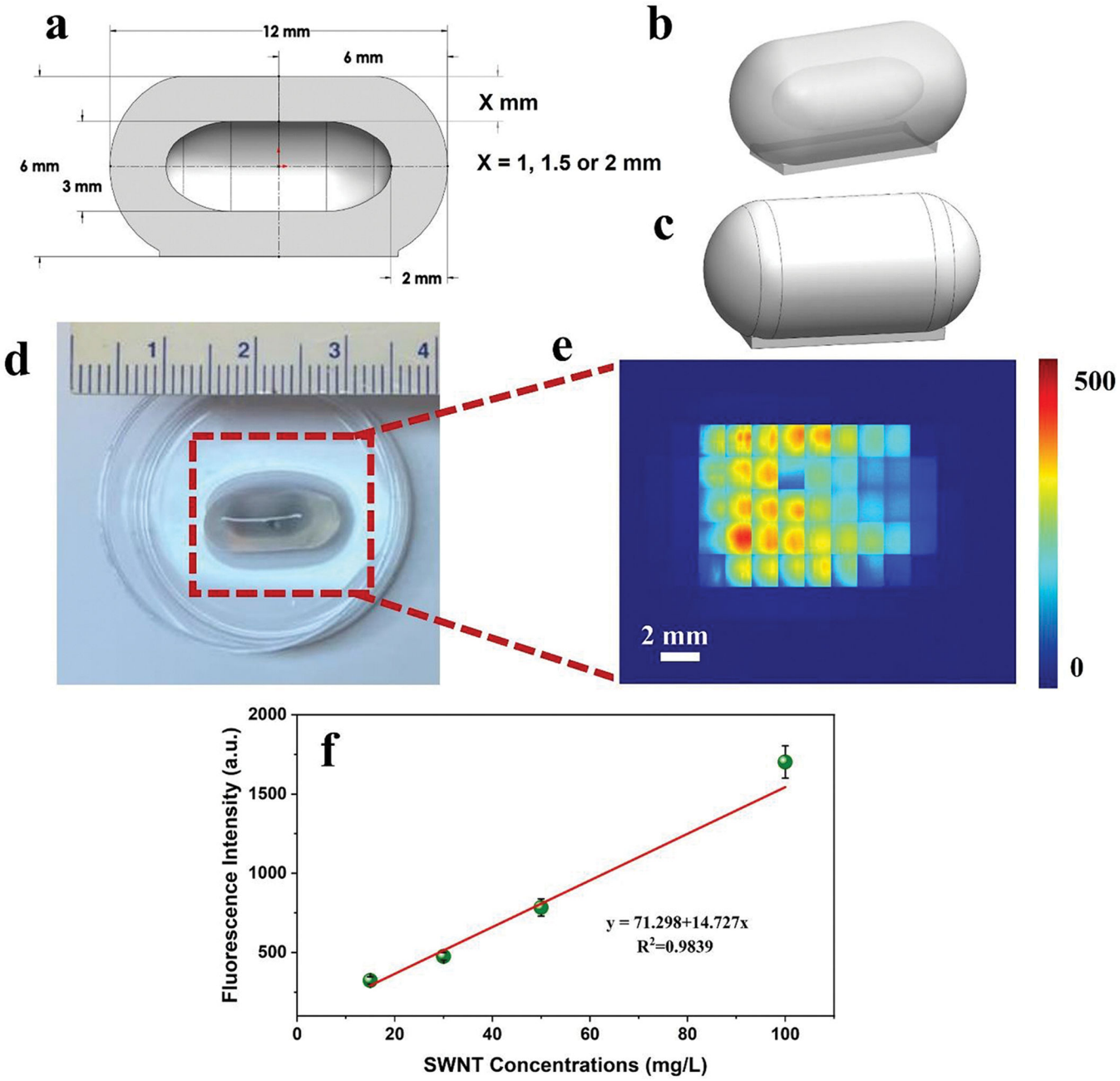

Fig. 2.

(**a**), (**b**), and (**c**) Schematic illustration of 3D printed liquid-core hydrogel design. (**d**) Digital image of a 30 mg/L of SWNT-loaded 1.5 mm thick liquid-core hydrogel sample and (**e**) its fluorescence image at 990 nm. (**f**) the linear correlation between the concentrations of SWNT loaded into the hydrogel (15, 30, 50, and 100 mg/L) and the fluorescence intensity

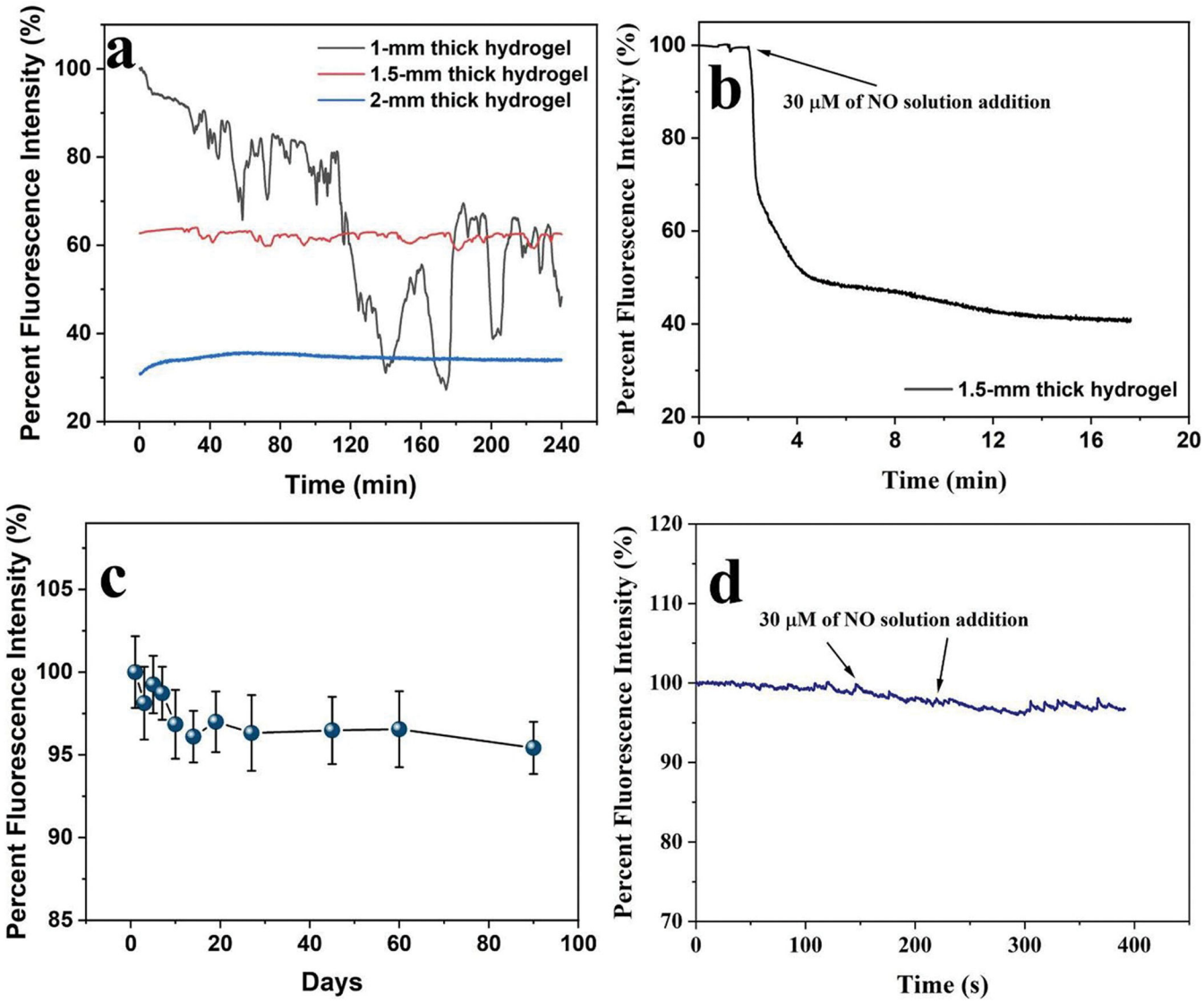

Fig. 3.

(**a**) Fluorescence stability of 1-, 1.5-, and 2-mm thick hydrogels over a 4-hour duration. (**b**) The $(AT)_{15}$-wrapped SWNT sensors in 1.5-thick hydrogels respond to the addition of 30 μM NO at 990 nm (final NO concentration is 10 μM). (**c**) Fluorescence stability of a 30 mg/L $(AT)_{15}$-wrapped SWNT loaded in a 1.5-mm thick hydrogel over 90 days. No statistical difference was found for any of the time points. (**d**) PVA-wrapped SWNTs in a 1.5-mm thick hydrogel did not respond to the addition of 30 μM NO

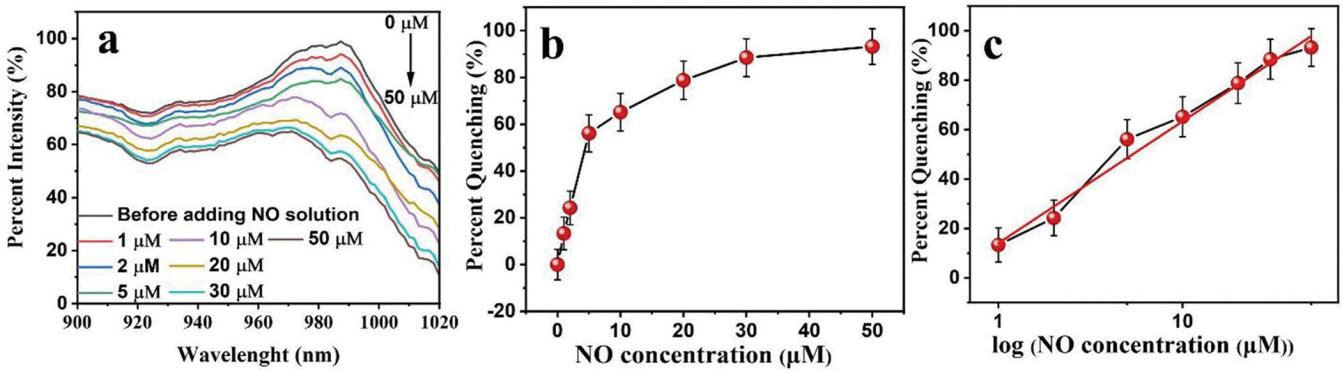

Fig. 4.

(**a**) The fluorescence spectral quenching upon the addition of various NO concentrations (0–50 μM) using 1.5-mm thick 30 mg/L SWNT-loaded hydrogels via an nIR spectrometer. (**b**) The corresponding fluorescence quenching of 1.5-mm thick 30 mg/L SWNT-loaded hydrogels at 990 nm from 0 μM to 50 μM (**c**) Linear fitting curve of the fluorescence quenching of the hydrogel at 990 nm towards the concentrations of NO from 1 μM to 50 μM

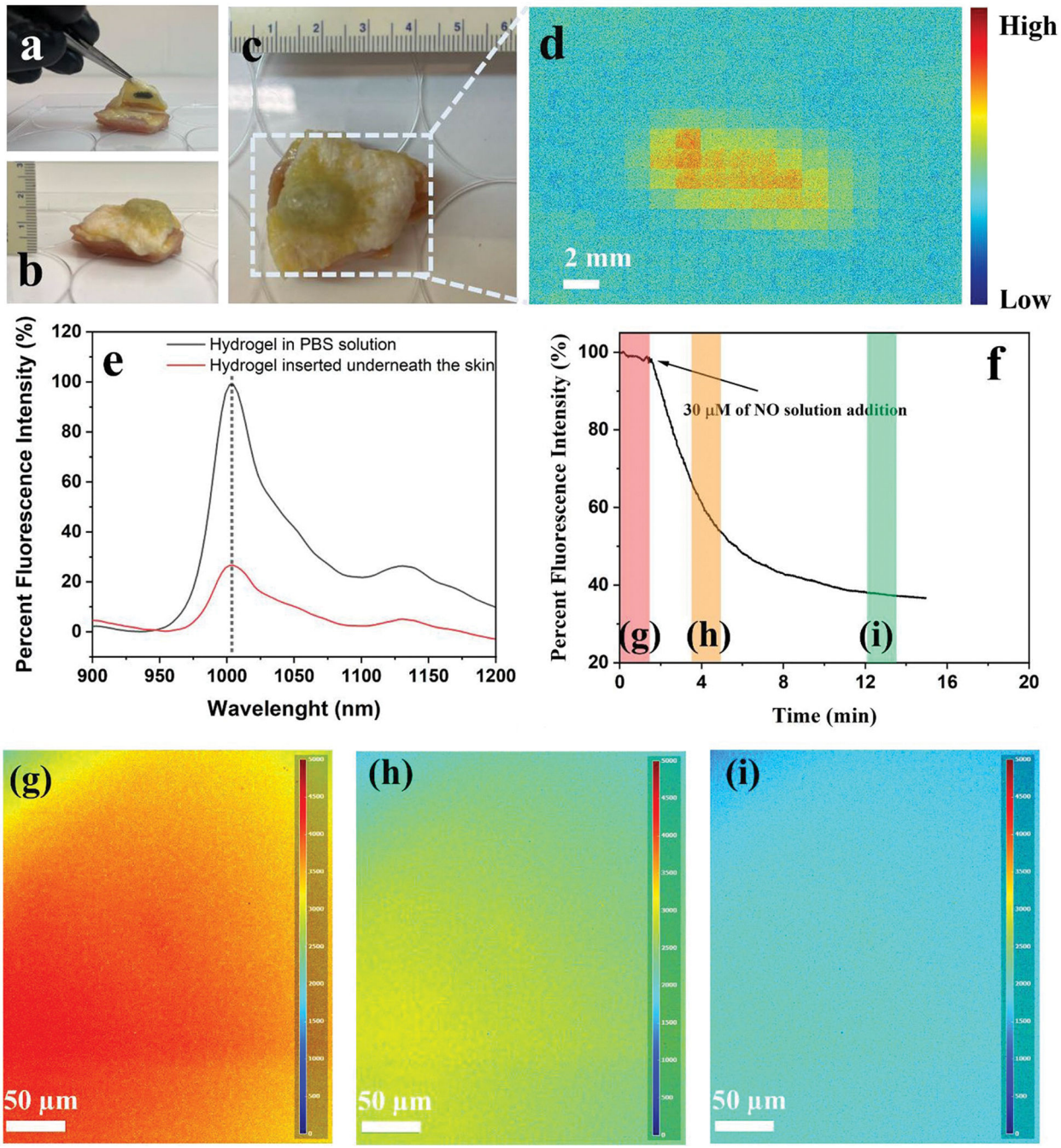

Fig. 5.

(**a**), (**b**), and (**c**) Digital images of the SWNT sensor-loaded liquid-core hydrogels inserted between the skin and muscle of a chicken breast and (**d**) the corresponding fluorescence intensity heat map. (**e**) Percent fluorescence spectra of (AT)15-wrapped SWNT sensor-loaded hydrogels before and after inserting them underneath the chicken skin (**f**) 1.5 mm-thick hydrogel response to the addition of 30 µM NO at 990 nm (final NO concentration is 10 µM) when it was inserted between the skin and muscle of a chicken breast and the

corresponding heat maps at different time points: (**g**) before, (**h**) during, and (**i**) after the quenching